Molecularly-informed field theories from bottom-up coarse-graining

Nicholas Sherck[1], Kevin Shen[1,2], My Nguyen[1], Brian Yoo[3], Stephan Köhler[4], Joshua Speros[5], Kris T. Delaney[2], M. Scott Shell[*,1], Glenn H. Fredrickson[*,1,2,6]

[1]Department of Chemical Engineering, University of California, Santa Barbara, California 93106 United States
[2]Materials Research Laboratory, University of California, Santa Barbara, California 93106 United States
[3]BASF Corporation, Tarrytown, New York, 10591, United States
[4]BASF SE, Ludwigshafen am Rhein 67056, Germany
[5]California Research Alliance (CARA) by BASF, Berkeley, California 94720, United States
[6]Department of Materials, University of California, Santa Barbara, California, 93106, United States

*Corresponding authors. Email: shell@ucsb.edu and ghf@mrl.ucsb.edu

ABSTRACT:

Polymer formulations possessing mesostructures or phase coexistence are challenging to simulate using atomistic particle-explicit approaches due to the disparate time and length scales, while the predictive capability of field-based simulations is hampered by the need to specify interactions at a coarser scale (e.g., χ-parameters). To overcome the weaknesses of both, we introduce a bottom-up coarse-graining methodology that leverages all-atom molecular dynamics to molecularly inform coarser field-theoretic models. Specifically, we use relative-entropy coarse-graining to parameterize particle models that are directly and analytically transformable into statistical field theories. We demonstrate the predictive capability of this approach by reproducing experimental aqueous polyethylene oxide (PEO) cloud-point curves with *no* parameters fit to experimental data. This synergistic approach to multiscale polymer simulations opens the door to *de-novo* exploration of phase behavior across a wide variety of polymer solution and melt formulations.

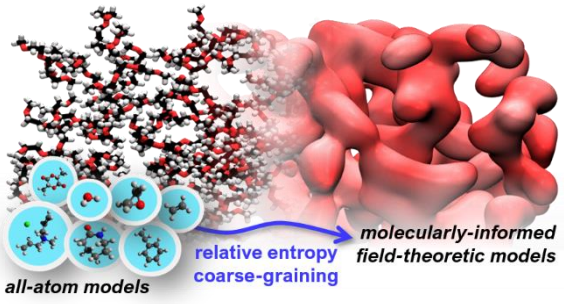

TOC Graphic

Complex polymer formulations are the basis for a vast range of important materials and products including paints, coatings, adhesives, cleaning and personal care products, elastomers, and plastics. To accelerate product design, improved methods for predictive modeling are greatly needed, specifically for sweeping the large, multivariate design space (polymer molecular weight, composition, architecture, and chemistry; solvent chemistry; solution composition; processing temperature; etc.) to explore resultant equilibrium structures and phases.[1] Characteristic of these systems are mesoscale structures spanning nanometer to micrometer length scales and long relaxation time scales associated with polymer diffusion and phase coarsening, reaching seconds, minutes, and even hours. While first principles and atomic-resolution particle simulations such as *ab-initio* molecular dynamics (MD) and classical atomistic MD methods are attractive for their predictive capabilities, they cannot access such large length and time scales and, consequently, have limited direct utility in formulation design.

Many efforts have instead turned to *bottom-up* coarse-graining strategies that map high-resolution atomistic models to coarser, effective "bead" models, sacrificing molecular detail for computational efficiency but retaining a connection to the underlying chemistry. There are many bottom-up, coarse-graining strategies including Boltzmann inversion,[2,3] force-matching,[4] and relative entropy coarse-graining,[5,6] among others,[7–10] with work demonstrating their applicability to a variety of soft matter classes that span small and large molecules alike.[7,11–16] However, the so-developed coarse-grained models are typically sampled using particle-based approaches (e.g., MD), which, despite the coarsening, inherently struggle to equilibrate systems at significantly larger times, such as those associated with large polymers capable of microphase or macrophase structuring on $\sim$1 μm scales. Furthermore, rigorous phase coexistence calculations are challenging and very often practically impossible even with coarse-grained particle representations due to the high computational cost of inserting (or deleting) macromolecules into (or from) dense phases.[17]

As an alternative to particle-based coarse-grained (CG) models, an equilibrium field-theoretic representation of the *identical* CG model circumvents the aforementioned challenges of constrained particle degrees of freedom by instead framing the model using auxiliary potential fields.[18,19] Field theories are particularly efficient when Angstrom scale features (e.g., liquid structuring) do not need to be resolved, instead capturing structural features in the nm range and above. Moreover, the number of polymers appears as a simple parameter in a field representation, so the computational expense becomes nearly independent of density. For this reason, field-theoretic simulations become much more efficient than particle MD at high polymer molecular-weight and/or high densities. Additionally, with a field representation molecular insertions (or deletions) involve simply changing a parameter in the field-theoretic model, enabling efficient and accurate Gibbs Ensemble Monte Carlo (GEMC) phase coexistence calculations even for macromolecules.[20,21] Contrarily, GEMC utilizing a particle

representation requires the development of complex schemes (e.g., configurational-bias[22–24] or continuous fractional component[25] Monte Carlo techniques, among many others[24,26,27]) to obtain reasonable acceptance for macromolecules of any appreciable size, particularly for liquid-liquid coexistence;[28] this is also the case even when "soft"-core interactions, like those found in dissipative particle dynamics, are utilized.[29–31]

Constructing a statistical field theory representation of a CG particle model involves the use of auxiliary potential fields to decouple non-bonded interactions in the model. Bonded interactions are embedded in single-chain propagator objects that track the statistics of single molecules subjected to the non-bonded auxiliary potential fields. Strategies for building field-theoretic models for broad classes of soft-matter systems have been detailed,[18] and such models have been the basis for a vast number of analytical and computational studies spanning block copolymer assembly,[32–39] polymeric emulsions,[40–44] polyelectrolyte complexation,[20,45–50] supramolecular assembly,[51–54] polymer nanocomposites[55,56] and colloidal interactions,[57] among others. An important practical limitation of field-theoretic representations is that they embed the emergent interactions of the underlying CG particle model and to date have relied upon phenomenological parameters with non-obvious connections to chemical details – most notably, Flory χ-parameters. This drawback has severely restricted their role as a predictive tool when encountering new chemistries.

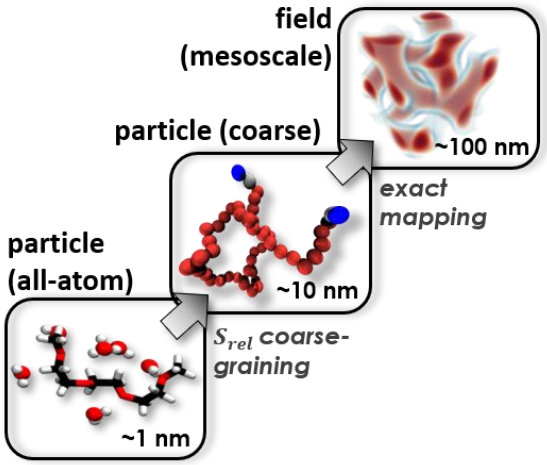

Figure 1. Relative-entropy coarse-graining serves as the bridge between the all-atom and the CG particle representations, while the latter is analytically converted to a field representation mathematically *identical* to the CG particle representation.

Here we introduce a new methodology that combines the strengths of both all-atom (AA) simulations and field theory, enabling truly predictive, bottom-up modeling of complex, large-scale systems while maintaining a direct connection to the underlying chemical design space, **Figure 1**. We overcome the phenomenological nature of field-theoretic models by obtaining chemically-informed parameters from small-scale, full-resolution, AA simulations. To bridge these methods, we use relative-entropy, S_{rel}, coarse-graining, a bottom-up approach that minimizes the information loss between a

reference microscopic configurational probability distribution, $\wp_{ref}(\boldsymbol{R})$, and that of the CG distribution, $\wp_{CG}(\boldsymbol{R})$: $S_{rel} = \int d\boldsymbol{R}\, \wp_{ref}(\boldsymbol{R}) \ln\left[\wp_{ref}(\boldsymbol{R})/\wp_{CG}(\boldsymbol{R})\right]$. The details of S_{rel} coarse-graining are discussed in the **SI** and have been reviewed in ref 6.

We adopt a CG force field, consisting of a harmonic bonding potential

$$\beta U_b(R) = k(R - R_o)^2 \qquad 1$$

where k and R_o are the bond stiffness and length, respectively, $\beta = (k_B T)^{-1}$, and nonbonded terms involving pairwise, repulsive Gaussian potentials often used in polymer field theory[58–60]

$$\beta U_{\alpha\gamma}(\boldsymbol{R}) = v_{\alpha\gamma} e^{-\boldsymbol{R}^2/4a_{\alpha\gamma}^2} \qquad 2$$

where $v_{\alpha\gamma}$ and $a_{\alpha\gamma}^2 = \left(a_\alpha^2 + a_\gamma^2\right)/2$ are the characteristic strength and range of the interaction between bead species α and γ, respectively. This functional form produces a microscopic model for n_p polymer molecules, each with N monomers, in a solvent of n_s molecules, that is readily written as a density-explicit statistical field theory[18] with a canonical partition function, Z_c, proportional to a functional integral over species density fields, $\boldsymbol{\rho}$, and auxiliary potential fields, $\boldsymbol{w}$, conjugate to the species densities

$$Z_c\left(n_p, n_s, V, T\right) \sim \int D\boldsymbol{w} \int D\boldsymbol{\rho}\, e^{-H[\boldsymbol{\rho},\boldsymbol{w}]} \qquad 3$$

Field configurations are weighted by the complex-valued, effective Hamiltonian, H

$$H[\boldsymbol{\rho},\boldsymbol{w}] = \frac{\beta}{2}\int d\boldsymbol{r} \int d\boldsymbol{r}'\, \boldsymbol{\rho}^T(\boldsymbol{r})\mathbf{U}(|\boldsymbol{r}-\boldsymbol{r}'|)\boldsymbol{\rho}(\boldsymbol{r}') - \int d\boldsymbol{r}\, i\boldsymbol{w}^T(\boldsymbol{r})\boldsymbol{\rho}(\boldsymbol{r}) - n_p lnQ_p\left[iw_p\right] - n_s lnQ_s[iw_s] \qquad 4$$

where $\mathbf{U}$ is a matrix of the through-space, non-bonded pair-interactions, and Q_p (Q_s) is the single chain (solvent molecule) partition function. The details of transforming from a particle to a density-explicit field representation is provided in the **Supporting Information** (**SI**).

We demonstrate this new methodology by calculating the temperature–composition, cloud-point curves of aqueous poly(ethylene oxide) (PEO, -CH_3 end-capped) solutions, one of the widest studied and industrially deployed water-soluble, synthetic polymer chemistries. We show in **Figure 2** the cloud-point curves for aqueous poly(ethylene glycol) (PEG, -OH end-capped) solutions measured from experiments by Bae *et al.*[61] and Saeki *et al.*[62], and note their closed-loop characteristic that are attributable to complex, temperature-dependent, ether-water interactions. At low temperatures outside the loops, PEG remains soluble, while at intermediate temperatures the ether-water hydrogen bonding weakens, leading to immiscibility and separation into polymer-rich and -lean phases. Finally, at higher temperatures the entropy of mixing favors reentrant homogenization. End-group chemistry does not affect the phase behavior of high-molecular weight chains[63,64] but does control the rate at which the loops close up with molecular weight. Dormidontova analyzed experimental data, finding the critical chain length of PEO to

be ~30 monomers, 20 lower than PEG (~50) with the difference dropping off inversely with chain length; notably, the critical temperature is essentially unaffected by the end-group chemistry.[65]

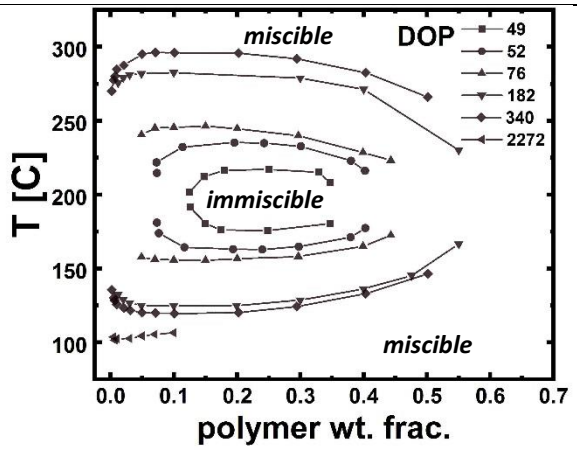

Figure 2. The experimentally measured, closed-loop, temperature-weight fraction cloud-point curves for aqueous PEG measured at varying degrees-of-polymerization (DOP) by Bae *et al.*[61] and Saeki *et al.*[62]

A number of studies have sought to interpret the closed-loop nature of the PEO cloud-point curves using analytical treatments, including pseudo-Flory-Huggins theories,[65–70] a statistical fluid theory for potentials of variable range (SAFT-VR),[71] and atomistic MD simulations coupled to thermodynamic modeling;[72] however, these efforts relied on fit parameter(s) from experimental data. In contrast, the present approach requires *no* fit parameters using experimental data, instead informing the field-theoretic model entirely from AA simulations. Specifically, we use the second-generation General Amber Force Field (GAFF2)[73,74] for PEO and the 4-site, Optimal Point Charge (OPC)[75] water model, for which we earlier found remarkably good agreement with experimental PEO conformations and temperature-composition-density behavior (see the **SI**).[76]

To parameterize field models, we collect reference AA MD trajectories for both neat water and neat PEO chains (20mers) at 25 °C and 1 atm, and for mixtures, at temperatures spanning 25-600 °C using small-scale ($n_w = 10{,}000$ and $n_p = 20$) AA simulations for 50mers at 0.20 polymer weight fraction. To remain faithful to the experimental PEO cloud-point measurement protocol, we equilibrate the mixtures at 25 °C and 1 atm (NPT), then fix the volume from the NPT equilibration at 25 °C during the production runs at elevated temperatures and, presumably, pressures, i.e., NVT;[72] further details of the AA simulations are provided in the **SI**.

To convert the reference AA trajectories to field-theoretic interaction parameters, we first start with pure species and then later determine mixture parameters. We map the AA trajectories onto the CG model's configuration space using a center-of-mass mapping for each water molecule and for each PEO monomer (-CH_2-O-CH_2-). Prior to S_{rel} optimization, we also determine the range of the nonbonded

interactions from the cube-root of the CG sites' specific volumes from analysis of the neat water and PEO reference simulations: $a_{ww} = v_w^{1/3} = 0.312$ nm and $a_{pp} = v_p^{1/3} = 0.375$ nm, which also determines $a_{pw} = \sqrt{0.5(a_{ww}^2 + a_{pp}^2)} = 0.345$ nm. While not unique, we find these choices for the coarse-grained mapping and non-bonded interaction potential ranges suppress the local liquid structure (**Figure 3, right**), which we do not seek to resolve with the field representation. S_{rel} coarse-graining in the NPT-ensemble ($P_{CG} = 113$ k_BT/nm^3 and $T = 25$ °C) yields the neat water-water and PEO-PEO interactions ($v_{ww} = 0.100$ & $v_{pp} = 0.430$) and the PEO bond strength and length ($k = 593$ nm^{-2} and $R_o = 0.324$ nm), while reproducing the AA models' neat solution densities well: $\rho_w = 1.02$ and $\rho_p = 1.10$ g/cm^3 (2% and 1.2% deviations from the AA model, respectively). Setting P_{CG} to 113 k_BT/nm^3 results in a CG water model ~3.0 times more compressible (1.26×10^{-4} bar^{-1}) than the AA water model (4.53×10^{-5} bar^{-1}) at 25 °C, while increasing P_{CG} further to 287 k_BT/nm^3 better matches the compressibility of water it minimally affects the phase-coexistence results (see **SI** for details). We use the CG pressure (P_{CG}) to control the overall strength of the interactions (specifying P_{CG} sets an energy scale); this approach has been used previously to generate entire families of CG models.[77] For simplicity, only the cross-interaction, $v_{pw}(T)$, is varied when coarse-graining the mixtures across temperature, **Figure 3 (left)**, while the like interactions and bonding parameters are held fixed; this restriction could be easily relaxed in future work to allow temperature dependence in all parameters. We find a four-parameter function, similar to forms used to fit χ-parameter data as a function of temperature,[78] interpolates the resultant $v_{pw}(T)$ data well, **Figure 3 (left, solid, red line**).

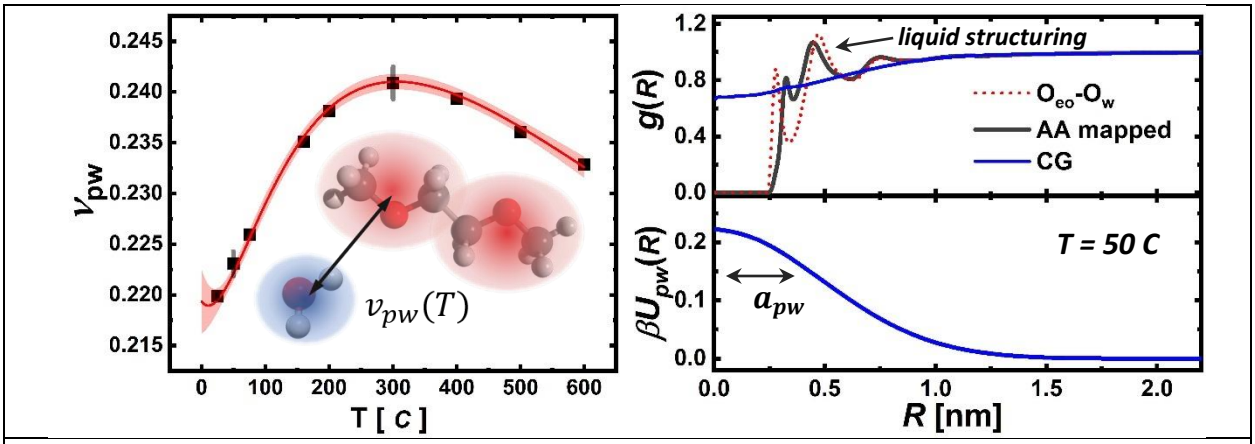

Figure 3. (left) The S_{rel} coarse-graining produces a complex, nonmonotonic temperature dependence of the PEO-water, $v_{pw}(T)$, interaction. The error bars for 25, 50 and 300 °C, represent 2 standard errors estimated from repeating the coarse-graining at least four times on the same all-atom (AA) reference trajectory. The solid red line is the fit from a four-parameter model to interpolate between the data points: $v_{pw}(T) = A + B/(T + 273) + C/(T + 273)^2 + D/(T + 273)^3$ (refer to the **SI** for the coefficients); the shaded region represents 90% confidence intervals on the fit. **(right)** The AA and CG radial distribution functions (AA $O_{eo} - O_{water}$ and mapped onto CG configuration space) and the $\beta U_{pw}(\boldsymbol{R})$ interaction at $N = 50, w_p = 0.20$, and $T = 50$ °C (see SI for 600 °C) . The CG model seeks to resolve only long length-scale physics and *not* short-length scale, liquid structuring still apparent even in the already coarsened (mapped), AA system.

To map out the binodal boundaries, we use the field representation in conjunction with a Gibbs ensemble approach[79] to accelerate the search for compositions that satisfy the equilibrium conditions, namely equality of chemical potentials and pressure across the two phases at a fixed temperature.[20,21,46] In general, this can be done approximation-free using field-theoretic simulations, or, as done here as a proof-of-concept, by making a mean-field approximation to the partition function in **eqn. 3**

$$\beta A(n_p, n_w, V, T) = -\ln Z \approx H[\boldsymbol{\rho}^*, \boldsymbol{w}^*] \qquad 5$$

where * denotes the mean-field configurations corresponding to a saddle point of H.[18] The precise mean-field expressions and the binodal (spinodal) calculation details are provided in the **SI**. A subtlety inherent to the cloud-point measurements is that the reported total density, ρ_o, at a specific polymer weight fraction, w_p, is fixed at conditions of 1 atm and 25 °C, since the samples were sealed in a vial before isochoric heating; thus, we set the total density accordingly, see **Figure 4 (right)** for $\rho_o(w_p)$.

The predicted PEO-water spinodal boundaries, **Figure 4 (left)**, capture the experimental PEO-water cloud-point curves semi-quantitatively, without *any* parameter refinement based on the experimental cloud-point data while using a remarkably simple functional form for U_{CG}, i.e., soft, repulsive Gaussian nonbonded and harmonic bonding interactions. The curves form closed loops of decreasing size with molecular weight and show a lower bound on PEO immiscibility at $N\sim3$, below which solubility stems from the increased translational entropy of the shorter chains. At higher molecular weights, the boundaries saturate on the polymer rich side to a weight fraction of ~0.53 ($T\sim300$ °C), near that of the experiments, ~0.58 ($T\sim195$ °C). The accuracy is notable because at the elevated temperatures the coarse-grained model is parameterized from a *single* reference composition ($w_p = 0.20$), with the like

interactions held temperature independent from coarse-graining the neat solutions at 25 °C and 1 atm; we also note that water's experimental activity in PEO at 25 °C and 1 atm is well reproduced from coarse-graining at this single composition and refer the interested reader to the **SI** for further details. The identifiable minimum (or maximum) temperatures at a fixed molecular weight, below (above) which phase separation does not occur, are also important signatures of the physical interactions. Their prediction with the multiscale workflow emerges entirely from the nonmonotonic temperature dependence of the PEO-water interaction (**Figure 3**). Notably, it appears to be necessary to capture the temperature dependence of only this *one* parameter (v_{pw}) at a single composition to produce the characteristic closed-loop cloud-point curves. The temperature dependence of v_{pw} encapsulates the complex, temperature-sensitive interplay between hydrogen-bonding (water-PEO and water-water) that competes with the systems translational entropy in dictating the miscibility gap.

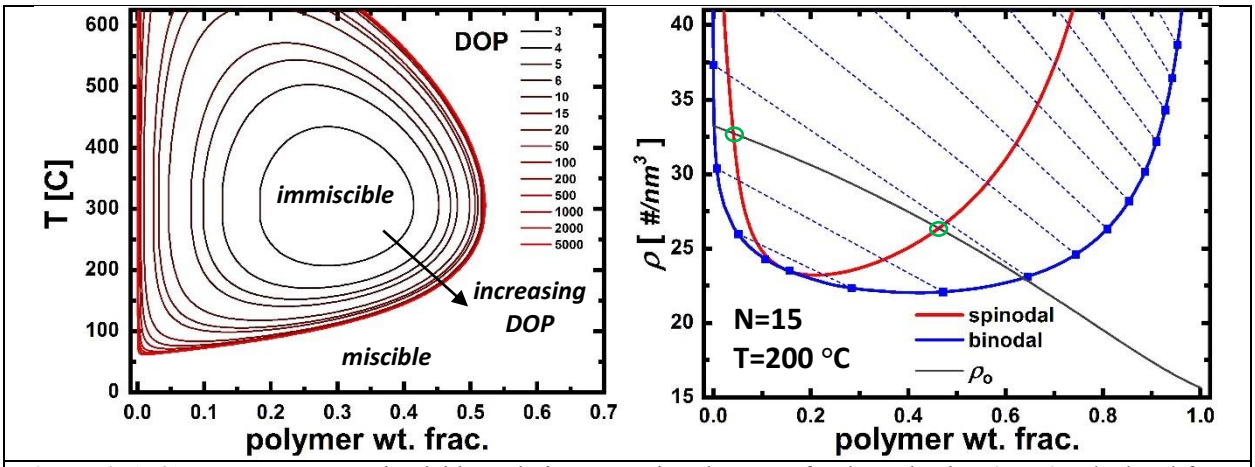

Figure 4. (left) Aqueous PEO, spinodal boundaries at varying degrees-of-polymerization (DOP) calculated from the field theory representation at the mean-field level. **(right)** The binodal with tie-lines (dashed) and spinodal boundaries at fixed DOP ($N = 15$) and temperature ($T = 200$ °C) as function of initial polymer weight fraction and the number density, ρ. The total number density, ρ_o, of the solution at room temperature and pressure is also overlaid (pure water ~33 waters/nm^3 whereas pure PEO ~15 monomers/nm^3). To construct the spinodal boundaries **(left)** one would read off the polymer weight fractions at the intersection of the ρ_o and spinodal curves **(right, green circles)**, and repeat at varying DOP and T.

The workflow admits two potential sources of error: (1) the accuracy of the AA force field for the target properties (here, phase coexistence boundaries), and; (2) CG model construction (e.g., choice of the mapping operator, the CG potential energy functional, and parameterization protocol) which directly affects the CG model transferability (in temperature and composition) and its overall fidelity relative to the underlying AA model. In other words, if the AA model were perfect and no loss of thermodynamic information occurred during the relative entropy-optimization, un-approximated sampling of the CG model would exactly replicate the self-assembly and thermodynamic properties of the AA model.

Regarding (1), AA force fields are continually undergoing refinement to increase their accuracy, and as this workflow is agnostic to the choice of the AA model, it is expected to only become more accurate with the availability of next-generation AA force fields. Similarly, errors of type (2) are the subject of intensive research in the bottom-up, coarse-graining community that we seek to altogether eliminate or systematically control.[80–82] While we do not endeavor to resolve both sources of error in this proof-of-concept demonstration of the workflow, we do investigate their impact on our predicted PEO solution miscibility. Specifically, we examine their influence on the temperature of maximum width, T_{mw}, of the cloud-point loops and on short-chain miscibility.

We find that T_{mw} is a strong function of the assigned atomic fixed charges of PEO in the AA model and that the CG model is sensitive to these fine interaction details. We examine the dependence of T_{mw} on the fixed charges using both a semi-empirical quantum calculation (AM1-BCC) with RESP charge fitting and by systematically scaling down the DFT assigned charges by just 5%. The AM1-BCC charge model yields a less polar PEO molecule and a larger v_{pw} (a lower solvent quality). Similarly, scaling down the B3LYP-obtained charges by just 5% increases v_{pw} (by 7% at $T = 300$ °C) resulting in larger loop diameters. Remarkably, this 5% decrease shifts the location of T_{mw} by 80 °C (from ~310 to ~230 °C), much nearer the experimentally observed value of ~195 °C (see **SI** for details). The dependence of miscibility on the atomic charges is expected, because these directly modulate the strength of hydrogen-bonding in the AA model, with a less polar PEO ether-backbone entailing a weaker hydrogen-bond with water, a larger v_{pw}, and phase separation at lower (higher) temperatures. Furthermore, the sensitivity to the AA force field is not unprecedented;[83] for example, in a dodecane/ethanol system a 1 kJ/mol difference in the transfer free energy (considered small during AA force field development) shifts the coexistence boundary by 50 °C.[28,84] Indeed, our CG model correctly captures trends in miscibility reflecting the changing solvent quality of the AA reference model–induced by changing PEO's atomic charges.

The second clear quantitative difference is immiscibility of shorter chains than is observed in experiments. By conducting a limited number of direct phase coexistence MD simulations of the AA (CG) model for low molecular-weight PEO solutions, we find evidence of phase separation for chains as short as ~6-10 (~4) monomers, whereas experimental data indicate full miscibility for $N \gtrsim 30$ (see **SI** for details).[65] Thus, we attribute a large portion–possibly the majority–of the difference in short chain miscibility to the AA reference model and not to the CG model construction.

In general, we expect the workflow's predictive accuracy to improve over time with methodological improvements from parallel lines of work. Starting at the bottom, higher resolution models are increasingly accurate as continued efforts focus on constructing improved classical AA force fields (e.g., polarizable or three-body force fields)[74,85–87], and as higher-level, *ab-initio* methods become

feasible at larger scales. Additionally, fidelity of the coarse-grained model to the AA reference model could be enhanced by considering: (1) more sophisticated functional forms for CG interactions, such as allowing for more complicated nonbonded interactions (e.g., repulsive, and attractive components) by representing each interaction using a Gaussian basis set, introducing arbitrary functional forms for bonding potentials (e.g., tabulated splines), or incorporating charges or polarization on the CG-sites; (2) a more systematic choice for the mapping between AA and CG representations, $\mathbf{M}(\boldsymbol{r})$, and of the length-scale(s) to resolve;[88–90] (3) the use of constraints during the S_{rel} minimization to better match target properties (e.g., Kirkwood-Buff Integrals[91] or R_g) from the AA model or–when available–experimental data,[92] and; (4) the choice of the ensemble to coarse-grain in, e.g., NPT, NVT or ensembles with external biasing potentials.[77,82,93]

In summary, we present here a broadly applicable, systematic bottom-up coarse-graining methodology utilizing all-atom simulations to molecularly-inform field-theoretic models that are well-suited to studying the mesoscopic, equilibrium properties of complex, polymeric solutions. Notably, our molecularly-informed functionals derive directly from the underlying CG particle model, not requiring the specification of basis functionals that support both expected and unanticipated mesoscale structure and thermodynamics; this is in contrast to the approach outlined by Invernizzi, *et al.* that inherently requires just such an *a-priori* specification for the phenomenological Hamiltonian functional.[93] We demonstrate the workflow's potential by constructing and parameterizing a molecularly-informed field theory for aqueous PEO, followed by a prediction for the solution's temperature-composition miscibility that directly connects the underlying polyether chemistry and hydrogen-bonding to macroscopic phase behavior. This multiscale approach is generalizable and readily extendable to a wide variety of industrially relevant soft-matter classes: multicomponent, charged, polarizable, macromolecular systems that can be spatially heterogenous at nanometer to micron length-scales, e.g., emulsions, complex coacervates, surfactant-micelle assemblies, polymer alloys, and block copolymers.

ASSOCIATED CONTENT

Supporting Information. Derivation of the field-theoretic model, binodal and spinodal boundary calculations, all-atom and coarse-grained simulation details, relative-entropy coarse-graining, effects of compressibility, $v_{pw}(T)$ dependence on PEO fixed-point charges, all-atom radial distribution functions, effects of fluctuations, and water activity data.

AUTHOR INFORMATION

ACKNOWLEDGEMENTS

This work was supported by BASF Corporation through the California Research Alliance. Use was made of computational facilities purchased with funds from the National Science Foundation (OAC-1925717) and administered by the Center for Scientific Computing (CSC). The CSC is supported by the California NanoSystems Institute and the Materials Research Science and Engineering Center (MRSEC; NSF DMR 1720256) at UC Santa Barbara. M.S.S. acknowledges funding support from the National Science Foundation through Award No. CHEM-1800344. G.H.F. and K.T.D. acknowledge support from the NSF CMMT Program under Award No. DMR-1822215. N.J.S would like to thank Clarke Palmer for insightful discussions and feedback.

REFERENCES

(1) Gartner, T. E.; Jayaraman, A. Modeling and Simulations of Polymers: A Roadmap. *Macromolecules* **2019**, *52* (3), 755–786. https://doi.org/10.1021/acs.macromol.8b01836.

(2) Müller-Plathe, F. Coarse-Graining in Polymer Simulation: From the Atomistic to the Mesoscopic Scale and Back. *ChemPhysChem* **2002**, *3* (9), 754–769. https://doi.org/10.1002/1439-7641(20020916)3:9<754::AID-CPHC754>3.0.CO;2-U.

(3) Lyubartsev, A. P.; Laaksonen, A. Calculation of Effective Interaction Potentials from Radial Distribution Functions: A Reverse Monte Carlo Approach. *Phys. Rev. E* **1995**, *52* (4), 3730–3737. https://doi.org/10.1103/PhysRevE.52.3730.

(4) Noid, W. G.; Chu, J. W.; Ayton, G. S.; Krishna, V.; Izvekov, S.; Voth, G. A.; Das, A.; Andersen, H. C. The Multiscale Coarse-Graining Method. I. A Rigorous Bridge between Atomistic and Coarse-Grained Models. *J. Chem. Phys.* **2008**, *128* (24), 11. https://doi.org/10.1063/1.2938860.

(5) Shell, M. S. The Relative Entropy Is Fundamental to Multiscale and Inverse Thermodynamic Problems. *J. Chem. Phys.* **2008**, *129* (14), 144108. https://doi.org/10.1063/1.2992060.

(6) Shell, M. S. Coarse-Graining with the Relative Entropy. In *Advances in Chemical Physics*; John Wiley & Sons, Inc., 2016; pp 395–441. https://doi.org/10.1002/9781119290971.ch5.

(7) Noid, W. G. Perspective: Coarse-Grained Models for Biomolecular Systems. *J. Chem. Phys.* **2013**, *139* (9), 090901. https://doi.org/10.1063/1.4818908.

(8) Noid, W. G. Systematic Methods for Structurally Consistent Coarse-Grained Models. *Methods Mol. Biol. Clifton NJ* **2013**, *924*, 487–531. https://doi.org/10.1007/978-1-62703-017-5_19.

(9) Guenza, M. G.; Dinpajooh, M.; McCarty, J.; Lyubimov, I. Y. Accuracy, Transferability, and Efficiency of Coarse-Grained Models of Molecular Liquids. *J. Phys. Chem. B* **2018**, *122* (45), 10257–10278. https://doi.org/10.1021/acs.jpcb.8b06687.

(10) Clark, A. J.; McCarty, J.; Lyubimov, I. Y.; Guenza, M. G. Thermodynamic Consistency in Variable-Level Coarse Graining of Polymeric Liquids. *Phys. Rev. Lett.* **2012**, *109* (16), 168301. https://doi.org/10.1103/PhysRevLett.109.168301.

(11) Wang, H.; Junghans, C.; Kremer, K. Comparative Atomistic and Coarse-Grained Study of Water: What Do We Lose by Coarse-Graining? *Eur. Phys. J. E* **2009**, *28* (2), 221–229. https://doi.org/10.1140/epje/i2008-10413-5.

(12) Villa, A.; Peter, C.; van der Vegt, N. F. A. Transferability of Nonbonded Interaction Potentials for Coarse-Grained Simulations: Benzene in Water. *J. Chem. Theory Comput.* **2010**, *6* (8), 2434–2444. https://doi.org/10.1021/ct100228t.

(13) Lebold, K. M.; Noid, W. G. Dual Approach for Effective Potentials That Accurately Model Structure and Energetics. *J. Chem. Phys.* **2019**, *150* (23), 234107. https://doi.org/10.1063/1.5094330.

(14) Harmandaris, V. A.; Adhikari, N. P.; van der Vegt, N. F. A.; Kremer, K. Hierarchical Modeling of Polystyrene: From Atomistic to Coarse-Grained Simulations. *Macromolecules* **2006**, *39* (19), 6708–6719. https://doi.org/10.1021/ma0606399.

(15) Ohkuma, T.; Kremer, K. A Composition Transferable and Time-Scale Consistent Coarse-Grained Model for Cis-Polyisoprene and Vinyl-Polybutadiene Oligomeric Blends. *J. Phys. Mater.* **2020**, *3* (3), 034007. https://doi.org/10.1088/2515-7639/ab906b.

(16) Sanyal, T.; Mittal, J.; Shell, M. S. A Hybrid, Bottom-up, Structurally Accurate, Go¯-like Coarse-Grained Protein Model. *J. Chem. Phys.* **2019**, *151* (4), 044111. https://doi.org/10.1063/1.5108761.
(17) Maerzke, K. A.; Siepmann, J. I. Transferable Potentials for Phase Equilibria−Coarse-Grain Description for Linear Alkanes. *J. Phys. Chem. B* **2011**, *115* (13), 3452–3465. https://doi.org/10.1021/jp1063935.
(18) Fredrickson, G. *The Equilibrium Theory of Inhomogeneous Polymers*; Oxford University Press on Demand, 2006.
(19) Fredrickson, G. H.; Ganesan, V.; Drolet, F. Field-Theoretic Computer Simulation Methods for Polymers and Complex Fluids. *Macromolecules* **2002**, *35* (1), 16–39. https://doi.org/10.1021/ma011515t.
(20) Danielsen, S. P. O.; McCarty, J.; Shea, J.-E.; Delaney, K. T.; Fredrickson, G. H. Molecular Design of Self-Coacervation Phenomena in Block Polyampholytes. *Proc. Natl. Acad. Sci.* **2019**, *116* (17), 8224–8232. https://doi.org/10.1073/pnas.1900435116.
(21) Riggleman, R. A.; Fredrickson, G. H. Field-Theoretic Simulations in the Gibbs Ensemble. *J. Chem. Phys.* **2010**, *132* (2), 024104. https://doi.org/10.1063/1.3292004.
(22) Frenkel, D.; Mooij, G. C. A. M.; Smit, B. Novel Scheme to Study Structural and Thermal Properties of Continuously Deformable Molecules. *J. Phys. Condens. Matter* **1992**, *4* (12), 3053–3076. https://doi.org/10.1088/0953-8984/4/12/006.
(23) Siepmann, J. I.; Frenkel, D. Configurational Bias Monte Carlo: A New Sampling Scheme for Flexible Chains. *Mol. Phys.* **1992**, *75* (1), 59–70. https://doi.org/10.1080/00268979200100061.
(24) de Pablo, J. J.; Bonnin, M.; Prausnitz, J. M. Vapor-Liquid Equilibria for Polyatomic Fluids from Site-Site Computer Simulations: Pure Hydrocarbons and Binary Mixtures Containing Methane. *Fluid Phase Equilibria* **1992**, *73* (3), 187–210. https://doi.org/10.1016/0378-3812(92)80010-7.
(25) Shi, W.; Maginn, E. J. Continuous Fractional Component Monte Carlo: An Adaptive Biasing Method for Open System Atomistic Simulations. *J. Chem. Theory Comput.* **2007**, *3* (4), 1451–1463. https://doi.org/10.1021/ct7000039.
(26) Bai, P.; Siepmann, J. I. Assessment and Optimization of Configurational-Bias Monte Carlo Particle Swap Strategies for Simulations of Water in the Gibbs Ensemble. *J. Chem. Theory Comput.* **2017**, *13* (2), 431–440. https://doi.org/10.1021/acs.jctc.6b00973.
(27) Rafferty, J. L.; Siepmann, J. I.; Schure, M. R. Retention Mechanism for Polycyclic Aromatic Hydrocarbons in Reversed-Phase Liquid Chromatography with Monomeric Stationary Phases. *J. Chromatogr. A* **2011**, *1218* (51), 9183–9193. https://doi.org/10.1016/j.chroma.2011.10.043.
(28) Harwood, D. B.; Peters, C. J.; Siepmann, J. I. A Monte Carlo Simulation Study of the Liquid–Liquid Equilibria for Binary Dodecane/Ethanol and Ternary Dodecane/Ethanol/Water Mixtures. *Fluid Phase Equilibria* **2016**, *407*, 269–279. https://doi.org/10.1016/j.fluid.2015.07.011.
(29) Liyana-Arachchi, T. P.; Jamadagni, S. N.; Eike, D.; Koenig, P. H.; Siepmann, J. I. Liquid–Liquid Equilibria for Soft-Repulsive Particles: Improved Equation of State and Methodology for Representing Molecules of Different Sizes and Chemistry in Dissipative

Particle Dynamics. *J. Chem. Phys.* **2015**, *142* (4), 044902. https://doi.org/10.1063/1.4905918.
(30) Minkara, M. S.; Hembree, R. H.; Jamadagni, S. N.; Ghobadi, A. F.; Eike, D. M.; Siepmann, J. I. A New Equation of State for Homo-Polymers in Dissipative Particle Dynamics. *J. Chem. Phys.* **2019**, *150* (12), 124104. https://doi.org/10.1063/1.5058280.
(31) Wijmans, C. M.; Smit, B.; Groot, R. D. Phase Behavior of Monomeric Mixtures and Polymer Solutions with Soft Interaction Potentials. *J. Chem. Phys.* **2001**, *114* (17), 7644–7654. https://doi.org/10.1063/1.1362298.
(32) Leibler, L. Theory of Microphase Separation in Block Copolymers. *Macromolecules* **1980**, *13* (6), 1602–1617.
(33) Fredrickson, G. H.; Helfand, E. Fluctuation Effects in the Theory of Microphase Separation in Block Copolymers. *J. Chem. Phys.* **1987**, *87* (1), 697–705. https://doi.org/10.1063/1.453566.
(34) Xie, N.; Li, W.; Qiu, F.; Shi, A.-C. σ Phase Formed in Conformationally Asymmetric AB-Type Block Copolymers. *ACS Macro Lett.* **2014**, *3* (9), 906–910. https://doi.org/10.1021/mz500445v.
(35) Kim, K.; Arora, A.; Lewis, R. M.; Liu, M.; Li, W.; Shi, A.-C.; Dorfman, K. D.; Bates, F. S. Origins of Low-Symmetry Phases in Asymmetric Diblock Copolymer Melts. *Proc. Natl. Acad. Sci.* **2018**, *115* (5), 847. https://doi.org/10.1073/pnas.1717850115.
(36) Zhao, M.; Li, W. Laves Phases Formed in the Binary Blend of AB4 Miktoarm Star Copolymer and A-Homopolymer. *Macromolecules* **2019**, *52* (4), 1832–1842. https://doi.org/10.1021/acs.macromol.8b02407.
(37) Lynd, N. A.; Oyerokun, F. T.; O'Donoghue, D. L.; Handlin, D. L.; Fredrickson, G. H. Design of Soft and Strong Thermoplastic Elastomers Based on Nonlinear Block Copolymer Architectures Using Self-Consistent-Field Theory. *Macromolecules* **2010**, *43* (7), 3479–3486. https://doi.org/10.1021/ma902517v.
(38) Lequieu, J.; Koeper, T.; Delaney, K. T.; Fredrickson, G. H. Extreme Deflection of Phase Boundaries and Chain Bridging in A(BA')n Miktoarm Star Polymers. *Macromolecules* **2020**, *53* (2), 513–522. https://doi.org/10.1021/acs.macromol.9b02254.
(39) Bates, M. W.; Lequieu, J.; Barbon, S. M.; Lewis, R. M.; Delaney, K. T.; Anastasaki, A.; Hawker, C. J.; Fredrickson, G. H.; Bates, C. M. Stability of the A15 Phase in Diblock Copolymer Melts. *Proc. Natl. Acad. Sci.* **2019**, *116* (27), 13194. https://doi.org/10.1073/pnas.1900121116.
(40) Broseta, D.; Fredrickson, G. H. Phase Equilibria in Copolymer/Homopolymer Ternary Blends: Molecular Weight Effects. *J. Chem. Phys.* **1990**, *93* (4), 2927–2938. https://doi.org/10.1063/1.458877.
(41) Bates, F. S.; Maurer, W. W.; Lipic, P. M.; Hillmyer, M. A.; Almdal, K.; Mortensen, K.; Fredrickson, G. H.; Lodge, T. P. Polymeric Bicontinuous Microemulsions. *Phys. Rev. Lett.* **1997**, *79* (5), 849–852. https://doi.org/10.1103/PhysRevLett.79.849.
(42) Fredrickson, G. H.; Bates, F. S. Design of Bicontinuous Polymeric Microemulsions. *J. Polym. Sci. Part B Polym. Phys.* **1997**, *35* (17), 2775–2786. https://doi.org/10.1002/(SICI)1099-0488(199712)35:17<2775::AID-POLB2>3.0.CO;2-Q.

(43) Düchs, D.; Ganesan, V.; Fredrickson, G. H.; Schmid, F. Fluctuation Effects in Ternary AB + A + B Polymeric Emulsions. *Macromolecules* **2003**, *36* (24), 9237–9248. https://doi.org/10.1021/ma030201y.
(44) Vorselaars, B.; Spencer, R. K. W.; Matsen, M. W. Instability of the Microemulsion Channel in Block Copolymer-Homopolymer Blends. *Phys. Rev. Lett.* **2020**, *125* (11), 117801. https://doi.org/10.1103/PhysRevLett.125.117801.
(45) Delaney, K. T.; Fredrickson, G. H. Theory of Polyelectrolyte Complexation—Complex Coacervates Are Self-Coacervates. *J. Chem. Phys.* **2017**, *146* (22), 224902. https://doi.org/10.1063/1.4985568.
(46) McCarty, J.; Delaney, K. T.; Danielsen, S. P. O.; Fredrickson, G. H.; Shea, J.-E. Complete Phase Diagram for Liquid–Liquid Phase Separation of Intrinsically Disordered Proteins. *J. Phys. Chem. Lett.* **2019**, *10* (8), 1644–1652. https://doi.org/10.1021/acs.jpclett.9b00099.
(47) Ermoshkin, A. V.; Olvera de la Cruz, M. A Modified Random Phase Approximation of Polyelectrolyte Solutions. *Macromolecules* **2003**, *36* (20), 7824–7832. https://doi.org/10.1021/ma034148p.
(48) Ghasemi, M.; Friedowitz, S.; Larson, R. G. Overcharging of Polyelectrolyte Complexes: An Entropic Phenomenon. *Soft Matter* **2020**. https://doi.org/10.1039/D0SM01466D.
(49) Qin, J.; de Pablo, J. J. Criticality and Connectivity in Macromolecular Charge Complexation. *Macromolecules* **2016**, *49* (22), 8789–8800. https://doi.org/10.1021/acs.macromol.6b02113.
(50) Shen, K.; Wang, Z.-G. Polyelectrolyte Chain Structure and Solution Phase Behavior. *Macromolecules* **2018**, *51* (5), 1706–1717. https://doi.org/10.1021/acs.macromol.7b02685.
(51) Lee, W. B.; Elliott, R.; Katsov, K.; Fredrickson, G. H. Phase Morphologies in Reversibly Bonding Supramolecular Triblock Copolymer Blends. *Macromolecules* **2007**, *40* (23), 8445–8454. https://doi.org/10.1021/ma071714y.
(52) Mohan, A.; Elliot, R.; Fredrickson, G. H. Field-Theoretic Model of Inhomogeneous Supramolecular Polymer Networks and Gels. *J. Chem. Phys.* **2010**, *133* (17), 174903. https://doi.org/10.1063/1.3497038.
(53) Mester, Z.; Lynd, N. A.; Delaney, K. T.; Fredrickson, G. H. Phase Coexistence Calculations of Reversibly Bonded Block Copolymers: A Unit Cell Gibbs Ensemble Approach. *Macromolecules* **2014**, *47* (5), 1865–1874. https://doi.org/10.1021/ma4026114.
(54) Fredrickson, G. H.; Delaney, K. T. Coherent States Field Theory in Supramolecular Polymer Physics. *J. Chem. Phys.* **2018**, *148* (20), 204904. https://doi.org/10.1063/1.5027582.
(55) Koski, J.; Chao, H.; Riggleman, R. A. Field Theoretic Simulations of Polymer Nanocomposites. *J. Chem. Phys.* **2013**, *139* (24), 244911. https://doi.org/10.1063/1.4853755.
(56) Koski, J. P.; Ferrier, R. C.; Krook, N. M.; Chao, H.; Composto, R. J.; Frischknecht, A. L.; Riggleman, R. A. Comparison of Field-Theoretic Approaches in Predicting Polymer Nanocomposite Phase Behavior. *Macromolecules* **2017**. https://doi.org/10.1021/acs.macromol.7b01731.
(57) Semenov, A. N. Theory of Colloid Stabilization in Semidilute Polymer Solutions. *Macromolecules* **2008**, *41* (6), 2243–2249. https://doi.org/10.1021/ma702536c.

(58) Delaney, K. T.; Fredrickson, G. H. Recent Developments in Fully Fluctuating Field-Theoretic Simulations of Polymer Melts and Solutions. *J. Phys. Chem. B* **2016**, *120* (31), 7615–7634. https://doi.org/10.1021/acs.jpcb.6b05704.
(59) Villet, M. C.; Fredrickson, G. H. Efficient Field-Theoretic Simulation of Polymer Solutions. *J. Chem. Phys.* **2014**, *141* (22), 224115. https://doi.org/10.1063/1.4902886.
(60) Wang, Z.-G. Fluctuation in Electrolyte Solutions: The Self Energy. *Phys. Rev. E* **2010**, *81* (2), 021501. https://doi.org/10.1103/PhysRevE.81.021501.
(61) Bae, Y. C.; Lambert, S. M.; Soane, D. S.; Prausnitz, J. M. Cloud-Point Curves of Polymer Solutions from Thermooptical Measurements. *Macromolecules* **1991**, *24* (15), 4403–4407. https://doi.org/10.1021/ma00015a024.
(62) Saeki, S.; Kuwahara, N.; Nakata, M.; Kaneko, M. Upper and Lower Critical Solution Temperatures in Poly (Ethylene Glycol) Solutions. *Polymer* **1976**, *17* (8), 685–689. https://doi.org/10.1016/0032-3861(76)90208-1.
(63) Spitzer, M.; Sabadini, E.; Loh, W. Poly(Ethylene Glycol) or Poly(Ethylene Oxide)?: Magnitude of End-Group Contribution to the Partitioning of Ethylene Oxide Oligomers and Polymers between Water and Organic Phases. *J. Braz. Chem. Soc.* **2002**, *13*, 7–9.
(64) Sadeghi, R.; Shahebrahimi, Y. Vapor−Liquid Equilibria of Aqueous Polymer Solutions from Vapor-Pressure Osmometry and Isopiestic Measurements. *J. Chem. Eng. Data* **2011**, *56* (4), 789–799. https://doi.org/10.1021/je100178s.
(65) Dormidontova, E. E. Influence of End Groups on Phase Behavior and Properties of PEO in Aqueous Solutions. *Macromolecules* **2004**, *37* (20), 7747–7761. https://doi.org/10.1021/ma035609+.
(66) Dormidontova, E. E. Role of Competitive PEO−Water and Water−Water Hydrogen Bonding in Aqueous Solution PEO Behavior. *Macromolecules* **2002**, *35* (3), 987–1001. https://doi.org/10.1021/ma010804e.
(67) Bekiranov, S.; Bruinsma, R.; Pincus, P. Solution Behavior of Polyethylene Oxide in Water as a Function of Temperature and Pressure. *Phys. Rev. E* **1997**, *55* (1), 577.
(68) Bae, Y. C.; Shim, J. J.; Soane, D. S.; Prausnitz, J. M. Representation of Vapor–Liquid and Liquid–Liquid Equilibria for Binary Systems Containing Polymers: Applicability of an Extended Flory–Huggins Equation. *J. Appl. Polym. Sci.* **1993**, *47* (7), 1193–1206. https://doi.org/10.1002/app.1993.070470707.
(69) Karlstroem, G. A New Model for Upper and Lower Critical Solution Temperatures in Poly(Ethylene Oxide) Solutions. *J. Phys. Chem.* **1985**, *89* (23), 4962–4964. https://doi.org/10.1021/j100269a015.
(70) Concentration Dependence of the Flory χ Parameter within Two-State Models | Macromolecules https://pubs.acs.org/doi/10.1021/ma020296o (accessed Mar 1, 2021).
(71) Clark, G. N. I.; Galindo, A.; Jackson, G.; Rogers, S.; Burgess, A. N. Modeling and Understanding Closed-Loop Liquid−Liquid Immiscibility in Aqueous Solutions of Poly(Ethylene Glycol) Using the SAFT-VR Approach with Transferable Parameters. *Macromolecules* **2008**, *41* (17), 6582–6595. https://doi.org/10.1021/ma8007898.
(72) Oh, S. Y.; Yang, H. E.; Bae, Y. C. Molecular Simulations and Thermodynamic Modeling for Closed-Loop Phase Miscibility of Aqueous PEO Solutions. *Macromol. Res.* **2013**, *21* (8), 921–930. https://doi.org/10.1007/s13233-013-1121-7.

(73) Wang, J.; Wolf Romain, M.; Caldwell James, W.; Kollman Peter, A.; Case David, A. Development and Testing of a General Amber Force Field. *J. Comput. Chem.* **2004**, *25* (9), 1157–1174. https://doi.org/10.1002/jcc.20035.
(74) He, X.; Man, V. H.; Yang, W.; Lee, T.-S.; Wang, J. A Fast and High-Quality Charge Model for the next Generation General AMBER Force Field. *J. Chem. Phys.* **2020**, *153* (11), 114502. https://doi.org/10.1063/5.0019056.
(75) Onufriev, A. V.; Izadi, S. Water Models for Biomolecular Simulations. *Wiley Interdiscip. Rev. Comput. Mol. Sci.* **2018**, *8* (2), e1347. https://doi.org/10.1002/wcms.1347.
(76) Sherck, N.; Webber, T.; Brown, D. R.; Keller, T.; Barry, M.; DeStefano, A.; Jiao, S.; Segalman, R. A.; Fredrickson, G. H.; Shell, M. S.; Han, S. End-to-End Distance Probability Distributions of Dilute Poly(Ethylene Oxide) in Aqueous Solution. *J. Am. Chem. Soc.* **2020**. https://doi.org/10.1021/jacs.0c08709.
(77) Lindquist, B. A.; Jadrich, R. B.; Howard, M. P.; Truskett, T. M. The Role of Pressure in Inverse Design for Assembly. *J. Chem. Phys.* **2019**, *151* (10), 104104. https://doi.org/10.1063/1.5112766.
(78) Knychała, P.; Timachova, K.; Banaszak, M.; Balsara, N. P. 50th Anniversary Perspective: Phase Behavior of Polymer Solutions and Blends. *Macromolecules* **2017**, *50* (8), 3051–3065. https://doi.org/10.1021/acs.macromol.6b02619.
(79) Panagiotopoulos, A. Z. Direct Determination of Phase Coexistence Properties of Fluids by Monte Carlo Simulation in a New Ensemble. *Mol. Phys.* **1987**, *61* (4), 813–826. https://doi.org/10.1080/00268978700101491.
(80) Dunn, N. J. H.; Foley, T. T.; Noid, W. G. Van Der Waals Perspective on Coarse-Graining: Progress toward Solving Representability and Transferability Problems. *Acc. Chem. Res.* **2016**, *49* (12), 2832–2840. https://doi.org/10.1021/acs.accounts.6b00498.
(81) Potter, T. D.; Tasche, J.; Wilson, M. R. Assessing the Transferability of Common Top-down and Bottom-up Coarse-Grained Molecular Models for Molecular Mixtures. *Phys. Chem. Chem. Phys.* **2019**, *21* (4), 1912–1927. https://doi.org/10.1039/C8CP05889J.
(82) Shen, K.; Sherck, N.; Nguyen, M.; Yoo, B.; Köhler, S.; Speros, J.; Delaney, K. T.; Fredrickson, G. H.; Shell, M. S. Learning Composition-Transferable Coarse-Grained Models: Designing External Potential Ensembles to Maximize Thermodynamic Information. *J. Chem. Phys.* **2020**, *153* (15), 154116. https://doi.org/10.1063/5.0022808.
(83) Boyd, N. J.; Wilson, M. R. Optimization of the GAFF Force Field to Describe Liquid Crystal Molecules: The Path to a Dramatic Improvement in Transition Temperature Predictions. *Phys. Chem. Chem. Phys.* **2015**, *17* (38), 24851–24865. https://doi.org/10.1039/C5CP03702F.
(84) Chen, Q. P.; Xie, S.; Foudazi, R.; Lodge, T. P.; Siepmann, J. I. Understanding the Molecular Weight Dependence of χ and the Effect of Dispersity on Polymer Blend Phase Diagrams. *Macromolecules* **2018**, *51* (10), 3774–3787. https://doi.org/10.1021/acs.macromol.8b00604.
(85) Jing, Z.; Liu, C.; Cheng, S. Y.; Qi, R.; Walker, B. D.; Piquemal, J.-P.; Ren, P. Polarizable Force Fields for Biomolecular Simulations: Recent Advances and Applications. *Annu. Rev. Biophys.* **2019**, *48* (1), 371–394. https://doi.org/10.1146/annurev-biophys-070317-033349.

(86) Cole, D. J.; Horton, J. T.; Nelson, L.; Kurdekar, V. The Future of Force Fields in Computer-Aided Drug Design. *Future Med. Chem.* **2019**, *11* (18), 2359–2363. https://doi.org/10.4155/fmc-2019-0196.
(87) Horton, J. T.; Allen, A. E. A.; Dodda, L. S.; Cole, D. J. QUBEKit: Automating the Derivation of Force Field Parameters from Quantum Mechanics. *J. Chem. Inf. Model.* **2019**, *59* (4), 1366–1381. https://doi.org/10.1021/acs.jcim.8b00767.
(88) Foley, T. T.; Shell, M. S.; Noid, W. G. The Impact of Resolution upon Entropy and Information in Coarse-Grained Models. *J. Chem. Phys.* **2015**, *143* (24), 243104. https://doi.org/10.1063/1.4929836.
(89) Chakraborty, M.; Xu, C.; White, A. D. Encoding and Selecting Coarse-Grain Mapping Operators with Hierarchical Graphs. *J. Chem. Phys.* **2018**, *149* (13), 134106. https://doi.org/10.1063/1.5040114.
(90) Foley, T. T.; Kidder, K. M.; Shell, M. S.; Noid, W. G. Exploring the Landscape of Model Representations. *Proc. Natl. Acad. Sci.* **2020**, *117* (39), 24061–24068. https://doi.org/10.1073/pnas.2000098117.
(91) Ganguly, P.; Mukherji, D.; Junghans, C.; van der Vegt, N. F. A. Kirkwood–Buff Coarse-Grained Force Fields for Aqueous Solutions. *J. Chem. Theory Comput.* **2012**, *8* (5), 1802–1807. https://doi.org/10.1021/ct3000958.
(92) Cesari, A.; Reißer, S.; Bussi, G. Using the Maximum Entropy Principle to Combine Simulations and Solution Experiments. *Computation* **2018**, *6* (1), 15. https://doi.org/10.3390/computation6010015.
(93) Invernizzi, M.; Valsson, O.; Parrinello, M. Coarse Graining from Variationally Enhanced Sampling Applied to the Ginzburg–Landau Model. *Proc. Natl. Acad. Sci.* **2017**, *114* (13), 3370–3374. https://doi.org/10.1073/pnas.1618455114.